J Mater Sci: Mater Electron (2023) 34:508

Effect of CdTe nucleation layer on the performance of CdS/CdTe thin film solar cells

G. K. U. P. Gajanayake[1], A. A. I. Lakmal[2], D. S. M. De Silva[1,*], and B. S. Dassanayake[2]

[1] *Department of Chemistry, University of Kelaniya, Kelaniya, Sri Lanka*
[2] *Department of Physics, University of Peradeniya, Peradeniya, Sri Lanka*

Received: 3 October 2022
Accepted: 15 January 2023
Published online: 11 February 2023

ABSTRACT

In this study, an electrodeposited CdTe nucleation layer (ED-CdTe*) was introduced on a chemical bath deposited (CBD) CdS layer prior to close-spaced sublimation (CSS) of the CdTe absorber layer to improve the efficiency of the CdS/CdTe solar cell by reducing the recombination mechanism in the depletion region. The ED-CdTe* nucleation layer grown in 40 s produced the highest efficiency of 9.12% with an open-circuit voltage (V_{OC}) of 640 mV, while the CBD-CdS/CSS-CdTe solar cell delivered 8.07% efficiency, with a V_{OC} of 596 mV. The ideality factor and the reverse saturate current density of the CBD-CdS/ED-CdTe*/CSS-CdTe solar cell were 2.28 and 6.65×10^{-5} mA/cm^2, respectively. After being treated with $CdCl_2$, the efficiency of the device with the nucleation layer (40 s) was elevated to 15.6% with a V_{OC} of 761 mV, and that of the device with no nucleation layer was raised up to 14.6% with a V_{OC} of 737 mV. Further, the solar cell with optimal ED-CdTe* nucleation layer showed the highest spectral response within the 400–900 nm wavelength range. The SEM and AFM analysis verified the formation of an ultrathin ED-CdTe* nucleation layer that can catalyse the film formation of CdTe by the CSS method while reducing the interface incongruity between CdS and CdTe layers.

1 Introduction

With the ever-increasing global population, the annual electricity consumption of the world is severely on the rise. Hence, using renewable energy sources has become an indispensable alternative, especially in adaptation to the use of solar power. Silicon and CdTe-based photovoltaic panels take the lead in power generation, although they have not yet reached their maximum theoretical efficiency of 32% [1, 2]. Among Si and CdTe-based photovoltaic panels, the CdS/CdTe panels still have a lower power conversion efficiency than other commercialised silicon panels. Nevertheless, CdS/CdTe solar cells receive great attention due to their low manufacturing cost and unperturbed device performance in the tropical climate.

Address correspondence to E-mail: sujeewa@kln.ac.lk

https://doi.org/10.1007/s10854-023-09895-6

The highest recorded power conversion efficiency to date of the CdS/CdTe solar cells was 22.1%, with its module efficiency of 18.6% [3, 4] for the device constructed by close-spaced sublimated (CSS) CdS and CdTe layers [3]. Though these CdS/CdTe solar modules were fabricated using a high-temperature physical vapour deposition technique, the manufacturing cost can be reduced if CdS is deposited using a chemical deposition technique. Therefore, many investigations are in progress using a blend of chemical and physical techniques to improve the efficiency of the CdS/CdTe solar cells while keeping the cost low.

Different deposition technique combinations were employed in CdS/CdTe cell development, such as both CdS and CdTe layers by electrodeposition (ED) [5] and by thermal evaporation [6, 7] chemical bath deposited CdS (CBD-CdS) with close-spaced vapour transport (CSVT) CdTe [8], CBD-CdS with thermal evaporated CdTe. In the present study, both chemical and physical deposition techniques were implicated in improving the performance of the CdS/CdTe solar cell. The chemical deposition techniques of CBD and ED were utilised to deposit the CdS window layer and CdTe nucleation layer, respectively, while the CdTe absorber layer was grown using the physical deposition technique of the CSS. Researchers have attempted to reduce recombination and shunting losses by introducing a ZnO buffer layer between the TCO and the CdS layer in the CdS/CdTe solar cells [9, 10].

In this work, CdTe nucleation (ED-CdTe*) was electrodeposited prior to the deposition of the CdTe absorber layer to mitigate the recombination effects in the CdS/CdTe solar cell. The nucleation layer grown in the p–n junction may improve the performance of the solar cell device by reducing the recombination between the window and absorber layer and increasing the number of carriers in the depletion region by maintaining the thickness of the nucleation layer within the depletion region. Furthermore, the CdTe nucleation layer may create a better substrate for the growth of the CSS-CdTe layer over the CBD-CdS layer, forming an ideal p–n junction to improve the performance of the photovoltaic device.

2 Materials and methods

2.1 Deposition of thin film CdS layer

The thin film CdS/CdTe solar cell was fabricated following the superstrate configuration on a fluorine-doped tin dioxide (glass/FTO) substrate. Before the deposition, substrates underwent a cleaning process with soaking in detergent followed by ultrasonication for 10 min. Then the substrates were immersed in acetone, methanol, and 2-propanol at 80 °C for 5 min in each. Afterwards, the cleaned glass/FTO substrates were dried and stored in a desiccator for later usage. Before the deposition of CBD-CdS, the substrates were subjected to a plasma cleaning process (Harrick Plasma PDC-002). In the chemical bath, 0.033 mol/L $Cd(CH_3COO)_2$ (Sigma-Aldrich, 99.99%), 0.667 mol/L $CS(NH_2)_2$ (Sigma-Aldrich, > 99.0%), $CH_3CO_2NH_4$ (Sigma-Aldrich, 99.99%) and concentrated NH_4OH (Sigma-Aldrich, ~ 25%) served as Cd and S precursors and pH adjusters, respectively. The deposition process adapted for CBD-CdS was a set of conditions optimised earlier [11]. After the growth of CBD-CdS thin film, samples were ultrasonicated and dried in N_2 airflow. Then, the CdS layer on the glass side was etched using diluted HCl and immediately rinsed under a DI water flow, subsequently placed on the hot plate at 100 °C for 5 min.

2.2 Deposition of ultrathin CdTe nucleation layer and CdTe absorber layers

The ultrathin ED-CdTe* layer was electrodeposited on the CBD-CdS layer. The three-electrode configuration consisted of a graphite sheet (counter electrode), saturated calomel electrode (reference electrode), and glass/FTO/CdS layer stack (working electrode) were immersed in the electrolyte prepared with 1.0 mol/L $CdSO_4$ and 1.0 mmol/L TeO_2 in pH 2.3 at 65 °C [12]. The ED-CdTe* layers were deposited at the deposition times of 20, 30, 40, 50, and 60 s to optimise the thickness of the nucleation layer. Hereafter the glass/FTO/CBD-CdS/ED-CdTe* samples prepared at varying deposition times of the nucleation layer were labelled as S 0, S 20, S 30, S 40, S 50 and S 60. Subsequently, the CdTe absorber layer was grown using the CSS technique. The substrate and the source temperatures were maintained at 580 °C and 640 °C, respectively. A separation of 4 mm was

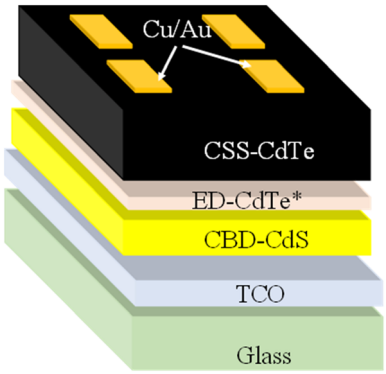

Fig. 1 Schematics of the glass/FTO/CBD-CdS/ED-CdTe*/CSS-CdTe

kept between the glass/FTO/CBD-CdS/ED-CdTe* substrates and the CdTe source for 25 min under argon ambience at a pressure of 7.9 Torr. Next, the glass/FTO/CBD-CdS/ED-CdTe*/CSS-CdTe samples were subjected to NP etching. Another set of samples was treated with $CdCl_2$ prior to the NP etching by following the wet $CdCl_2$ treatment process [13]. Therein, 1 mol/L $CdCl_2$ was sprayed over samples and annealed at 390 °C for 10 min. Finally, Cu/Au back contact (0.087 cm^2) was fabricated using the thermal evaporation technique and annealed in N_2 ambient at 200 °C for 20 min to complete the device structure of glass/FTO/CBD-CdS/ED-CdTe*/CSS-CdTe shown schematically in Fig. 1.

2.3 Characterisation

The absorbance and transmittance spectra of glass/FTO/CBD-CdS/ED-CdTe* and glass/FTO/CSS-CdTe samples were obtained by a UV–visible spectrophotometer (PerkinElmer UV/VIS Lambda 365) within the wavelength range of 300–900 nm. The elemental composition of the glass/FTO/CSS-CdTe sample was analysed by X-ray fluorescence (XRF) spectrometer (Bruker S8 TIGER Series 2-WDXRF elemental analysis system) to identify the conductive type by studying the composition of Cd and Te in the CSS-CdTe material before and after the $CdCl_2$ treatment. The electrical properties of the fabricated devices were measured under illuminated [AM 1.5 (1000 W/cm^2)] and dark conditions using the solar simulator (PEC—L12). The spectral responses of the devices were also measured using a lock-in amplifier (Stanford Research-SR 830 DSP) consisting of a monochromator (ScienTcetech 9010) and a chopper (Stanford-SR 540) at the frequency of 63 Hz. The morphology and cross-sectional view of the glass/FTO/CBD-CdS/ED-CdTe* and the glass/FTO/ED-CdTe* were obtained using a scanning electron microscope (SEM, Hitachi SU6600). AFM analysis (Park systems-XE7, Suwon-si) was performed on glass/FTO/CBD-CdS and optimised glass/FTO/CBD-CdS/ED-CdTe* sample.

3 Results and discussion

3.1 Optical properties

The optical transmittance and the Tauc plots of glass/FTO/CBD-CdS/ED-CdTe* layer stacks grown, varying the deposition time of ED-CdTe*, are shown in Fig. 2a and b, respectively. Herein, the sample deposited without nucleation layer (S 0) has shown over 80% transmission of light in the wavelength range of 520–900 nm, and the samples S 20, S 30 and S 40 have shown a similar transmittance in a slightly narrow optical window (535–900 nm), while S 50 and S 60 transmit in a further narrowed optical window (570–900 nm). Accordingly, the nucleation layer of the samples S 20, S 30, and S 40 do not obstruct the light absorbance.

Table 1 and Fig. 2 show that the energy bandgap (E_g) of samples S 0 to S 60 declined from 2.39 to 2.35 eV. Herein, the CdTe nucleation layer in S 20, S 30 and S 40 has not been affected much in light transmittance (E_g = 2.37 eV) through the structure, glass/FTO/CBD-CdS/ED-CdTe*, whilst working as a minimum light absorber. In contrast, the samples of S 50 and S 60 show higher light absorbance. This envisages the ability of such a nucleation layer (S 20–S 40) as an efficient substrate for the growth of the p-CdTe absorber layer.

Figure 3a and b shows the transmittance and the Tauc plots corresponding to the CSS-CdTe absorber material. As in the Tauc plot, the energy band gap calculated for the CSS-CdTe absorber layer was 1.49 eV. Further, it has shown less transmittance within a wavelength range (400–820 nm) and was transmitted less than 30% up to 1100 nm. Therefore, more incident radiations were absorbed, both in the solar spectrums' visible (∼ 380–700 nm) and in the IR region (∼ 700 nm−1 mm). The p-type conductivity of the CSS-CdTe was confirmed by the XRF data providing the Te-rich nature with 25.4% Cd and 74.6% Te in the CSS-CdTe material. The Te richness

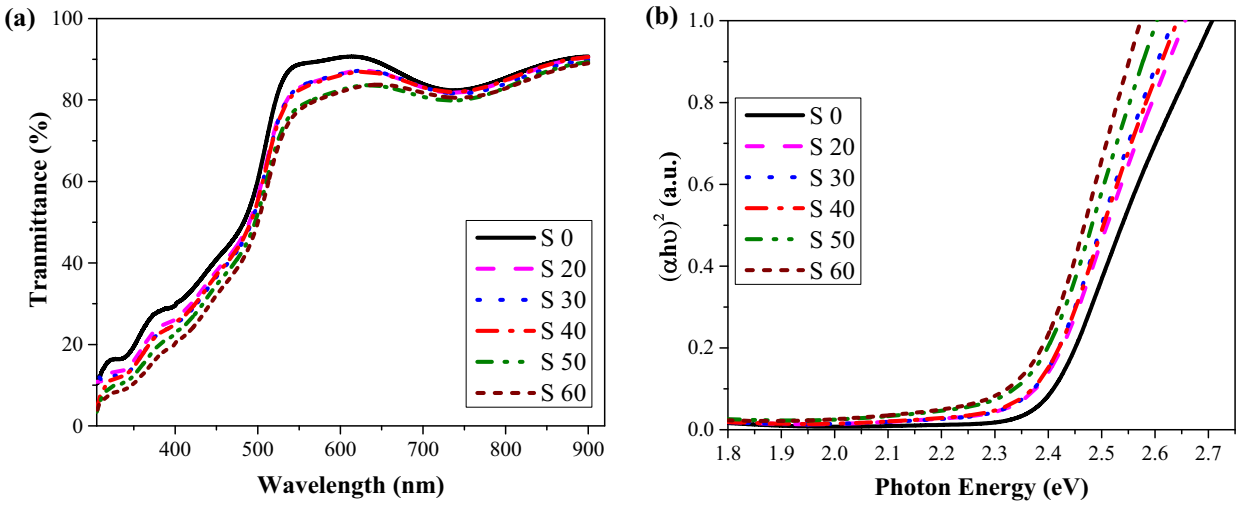

Fig. 2 **a** The transmittance vs. wavelength variation and **b** Tauc plots of the glass/FTO/CBD-CdS/ED-CdTe* samples grown by varying the deposition time of the nucleation layer

Table 1 The energy band gap of the glass/FTO/CBD-CdS/ED-CdTe* samples

Sample	S 0	S 20	S 30	S 40	S 50	S 60
Deposition duration of ED-CdTe* layer (s)	0	20	30	40	50	60
The energy band gap (eV)	2.39	2.37	2.37	2.37	2.36	2.35

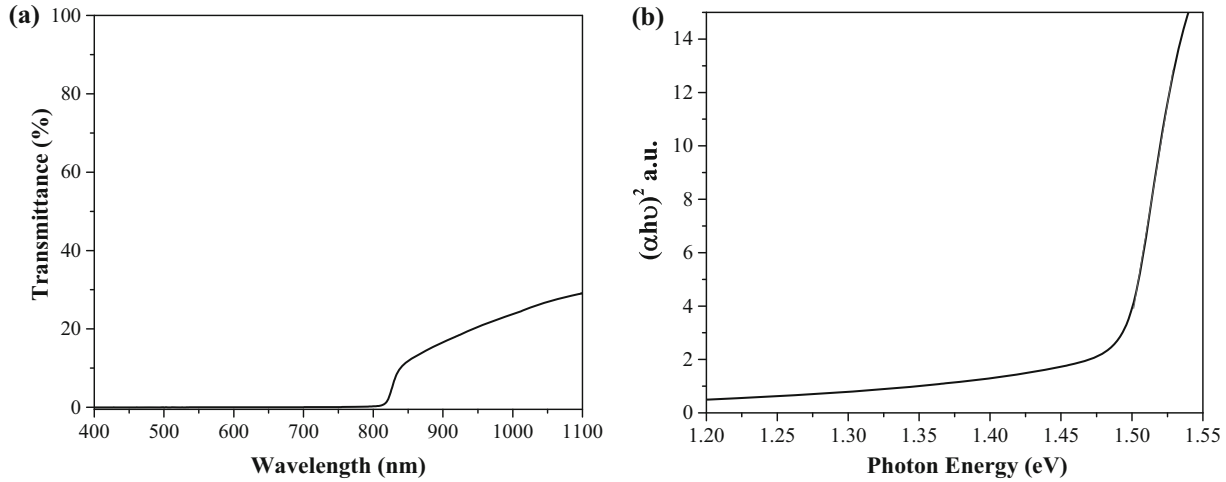

Fig. 3 **a** Transmittance vs. wavelength plot and **b** Tauc plot for CSS-CdTe absorber layer

of the CdTe material ensured in the formation of p-type CdTe, and Cd richness results in n-type CdTe [14].

3.2 Device performance

The performance of the glass/FTO/CBD-CdS/ED-CdTe*/CSS-CdTe/Cu/Au solar cells (referred to as SC 0, SC 20, SC 30, SC 40, SC 50, SC 60, cell area—0.087 cm^2) are tabulated in Table 2. As given in Table 2, the power conversion efficiencies (PCE) of SC 20-SC 60 were found to be higher than that of SC 0. The cell SC 40 delivered the highest conversion efficiency of 9.1%, with a short circuit current density (J_{SC}) of 30.3 mA/cm^2, open-circuit voltage (V_{OC}) of 640 mV, and an *FF* of 47%. It is a 13% improvement in conversion efficiency of the CdS/CdTe solar cells implanted with ED-CdTe* nucleation layer (SC 40)

Table 2 Performance of the CdS/CdTe solar cells

Sample	SC 0	SC 20	SC 30	SC 40	SC 50	SC 60
J_{SC} (mA/cm^2)	30.9	28.6	29.0	30.3	27.9	29.2
V_{OC} (V)	0.596	0.638	0.661	0.640	0.646	0.664
FF (%)	44	46	45	47	47	44
PCE (%)	8.1	8.3	8.6	9.1	8.4	8.6
R_s (Ω)	70.2	68.6	60.4	62.3	64.4	67.4
R_{sh} (Ω)	646.0	688.1	658.5	723.4	731.5	646.6

than the CdS/CdTe solar cell with no nucleation layer (SC 0).

Then SC 30 and the SC 60 cells lined up next in terms of efficiency while delivering the higher V_{OC} among the series. With the implantation of the ED-CdTe* nucleation layer, the solar cells' series resistance tends to reduce, while the V_{OC} values tend to be higher compared to the cell with no nucleation layer. This can be attributed to improved contact between the CdS window layer and the CdTe absorber layer via the ED-CdTe*. Figure 4 shows the variation of V_{OC} and the J_{SC} under 1.5 AM illumination of each cell developed.

The current density of the solar cells was measured by applied voltage in the dark at room temperature. The semilog linear J–V characteristics curve of the solar cells in the dark is shown in Fig. 5. Then, the ideality factor and the reverse saturation current density of the FTO/CBD-CdS/CSS-CdTe and FTO/CBD-CdS/ED-CdTe*/CSS-CdTe solar cells were

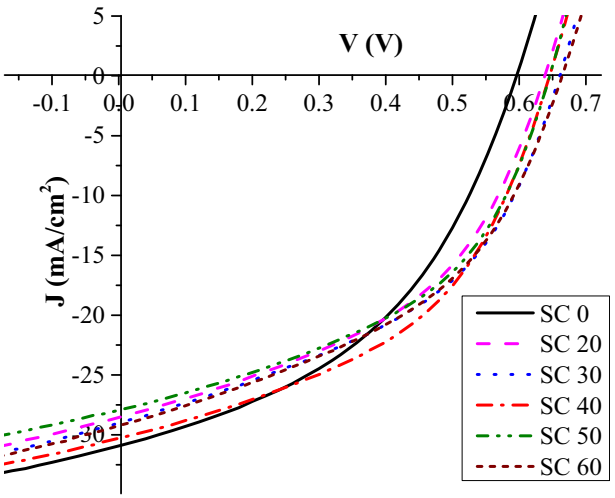

Fig. 4 J–V curves of the CdS/CdTe solar cells under illumination for SC 0 to SC 60

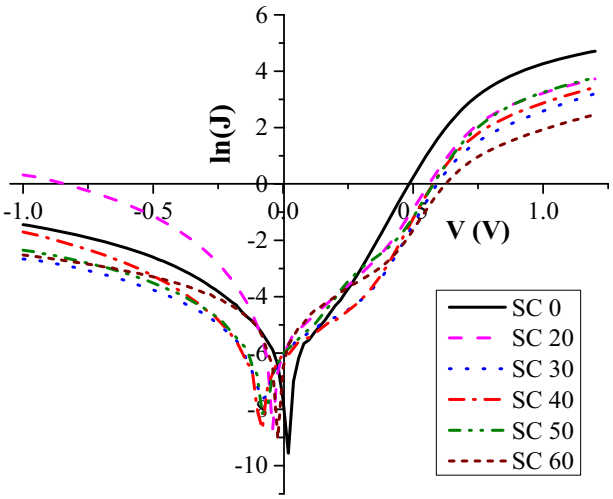

Fig. 5 The semi-log linear J–V characteristics curve under the dark condition for S 0 to S 60

calculated by considering the linear region of the semilog-linear J–V curve. The gradient determines the ideality factor, and the intercept gives the reverse saturation current density, as represented in Eq. 2 [15]. The current density of a solar cell under the dark condition is provided by Eq. 1, where J_0 is reverse saturation current, n is the ideality factor, k is Boltzmann's constant, and T is the absolute temperature. The series resistance R_s of the device are assumed to be negligible [16].

$$J = J_o\left\{\exp\left[\frac{q(V - JR_s)}{nkT}\right] - 1\right\} \tag{1}$$

$$\ln J = \frac{q(V - JR_s)}{nkT} + \ln J_o$$

$$\ln J = \frac{qV}{nkT} + \ln J_o \tag{2}$$

The n and J_0 are the best parameters for understanding the performance of a solar cell. The reverse saturation current density originates from minority carriers in the p–n junction, representing the recombination mechanism in a solar cell. When the J_0 is increased, the e–h recombination also increases; hence, the photo-generated charge carriers' density decreases [17]. The possible recombination mechanisms that occur in semiconductors are known as radiative (band to band) recombination, Auger recombination, and Shockley–Read–Hall (SRH) recombination. [18]. In the band-to-band recombination mechanism, the electrons in the conduction band recombine with holes in the valence band, releasing

photons as energy. In Auger recombination, electrons combine with the holes, which releases energy; simultaneously, this energy is transferred to another electron to excite to a higher position in the conduction band. This excited electron then returns to the conduction band edge, releasing its energy as thermal. Among the mechanisms mentioned above, SRH recombination is dominant due to defect states in semiconductor materials. Herein, the electrons in the conduction band move to the extra energy levels in the forbidden band and further move to the valence band to combine with holes by releasing energy as photons or phonons [17, 18].

In this study, as the calculated n values for the cell series, the lowest value of 2.28 was from SC 40, while the highest 2.76 was observed in SC 50 (Table 3). In an ideal solar cell, the n is equal to one. Hence, the higher values of the ideality factor ($n > 1$) reflect more recombination and the presence of defects in the device [19]. If the n is closer to 3, the Auger recombination could be dominated over SRH recombination and the band-to-band recombination mechanisms [15]. Therefore, the lowest n value in this study, which was recorded for the ED-CdTe* nucleation layer grown for 40 s, suggests that it has a thickness good enough to minimise the recombinations between the CBD-CdS and CSS-CdTe layers. Although the SC 60 has shown the third highest efficiency, its n is also high, which implies the occurrence of detrimental recombinations in the device, limiting its efficiency. Further, the SC 60, having the thickest nucleation layer, may accompany higher defect states. Therefore, that can promote some electrons to excite by absorbing thermal energy (IR) in its surrounding during its passage leading to higher efficiency despite its high ideality factor [19, 20].

Therefore, it can be concluded that the nucleation layer formed in this study is in favour of enhancing the device's efficiency while acting as a compatible substrate to accommodate the sublimated CdTe. In thin film solar cells, the ED-CdTe were reported to be in columnar structures [21–23], but lower deposition times used in this study prevented such formations and resulted in ultrathin CdTe layers. Hence, the substrate structure is in favour of preventing void formation during the sublimation of the CSS-CdTe absorber layer [24].

Further, based on the above results, the devices SC 30 and SC 40 with the lowest n were selected for further investigations.

3.3 Spectral response

The spectral response of each FTO/CBD-CdS/ED-CdTe*/CSS-CdTe solar cell is depicted in Fig. 6. The solar cell SC 40 shows the highest photo response within the 400–850 nm wavelength range (UV and near IR), while the other devices have shown a gradual decrease in their photo response with decreasing the thickness of the CdTe nucleation layer. The lower spectral response of SC 20 and SC 30 in the short wavelength range could be due to higher recombination at the front surface [25]. In addition, the device SC 60 exhibits a low spectral response in the long-wavelength region, which may indicate the high recombination at the back surface. The SC 40 has

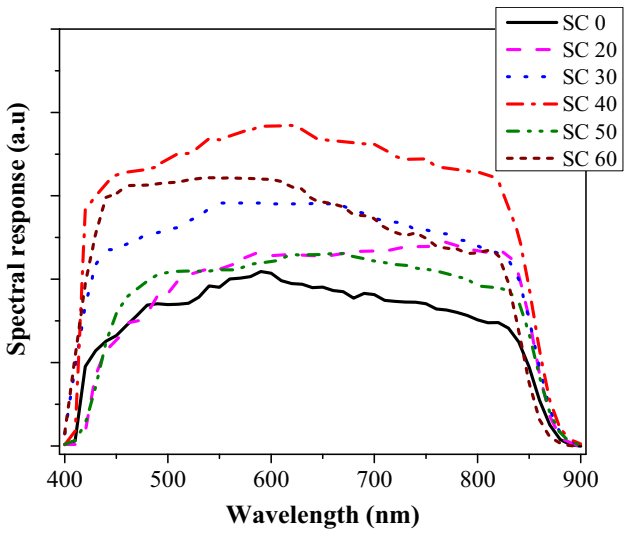

Fig. 6 Normalized spectral response for the FTO/CBD-CdS/CSS-CdTe and FTO/CBD-CdS/ED-CdTe*/CSS-CdTe solar cell devices within the wavelength range of 400–900 nm

Table 3 The n and J_0 of the CBD-CdS/CSS-CdTe and CBD-CdS/ED-CdTe*/CSS-CdTe solar cells

Sample	SC 0	SC 20	SC 30	SC 40	SC 50	SC 60
n	2.41	2.70	2.35	2.28	2.76	2.74
J_0 (mA/cm^2)	4.37×10^{-4}	3.40×10^{-4}	6.71×10^{-5}	6.65×10^{-5}	3.06×10^{-4}	1.80×10^{-4}

shown lower surface recombination than the other samples, with a high spectral response within the entire wavelength range of 400–850 nm. A significant portion of the charge carriers may involve in the recombination process, reducing the mobile charge carrier density and hence mitigating the device's performance.

3.4 Scanning electron microscope (SEM) analysis

Figure 7a shows the cross-sectional view under the SEM of the FTO/CBD-CdS/ED-CdTe* sample with the nucleation layer grown for 40 s, and Fig. 7b depicts ED-CdTe* layer grown under the same conditions but on bare FTO substrate. According to Fig. 7a, the average thickness of the CBD-CdS/ED-CdTe* layer was ~ 102 nm. Figure 7a and b further depicted that the ED-CdTe* nucleation layer is nicely fused with the CBD-CdS layer making no borderline. Hence, the ED-CdTe* is readily available to accommodate the sublimated CdTe absorber layer homogeneously. Since the ultrathin nature of the ED-CdTe* layer, it can stay inside the depletion region of the CBD-CdS/CSS-CdTe junction. Figure 8a and b shows the surface morphology of a bare CBD-CdS and b CBD-CdS/ED-CdTe* corresponded to S 40. The tinny grains of the nucleation layer appeared, filling the voids in the CdS substrate, and creating a compact layer.

Figure 9a shows the AFM images of bare CBD-CdS, and Fig. 9b corresponds to sample S 40. This is further evidence of the growth of a well-compact nucleation layer of CdTe in sample S 40. Hence, both SEM and AFM evident the uniform growth of grains over the CBD-CdS forming a compacted substrate.

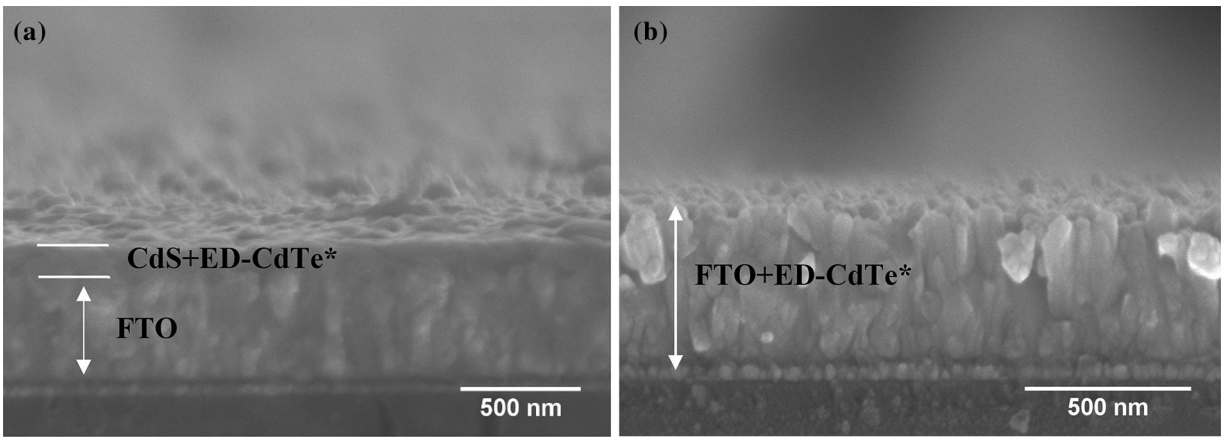

Fig. 7 The cross section of the sample S 40 **a** FTO/CBD-CdS/ED-CdTe*(S 40) and **b** FTO/ED-CdTe* grown for 40 s

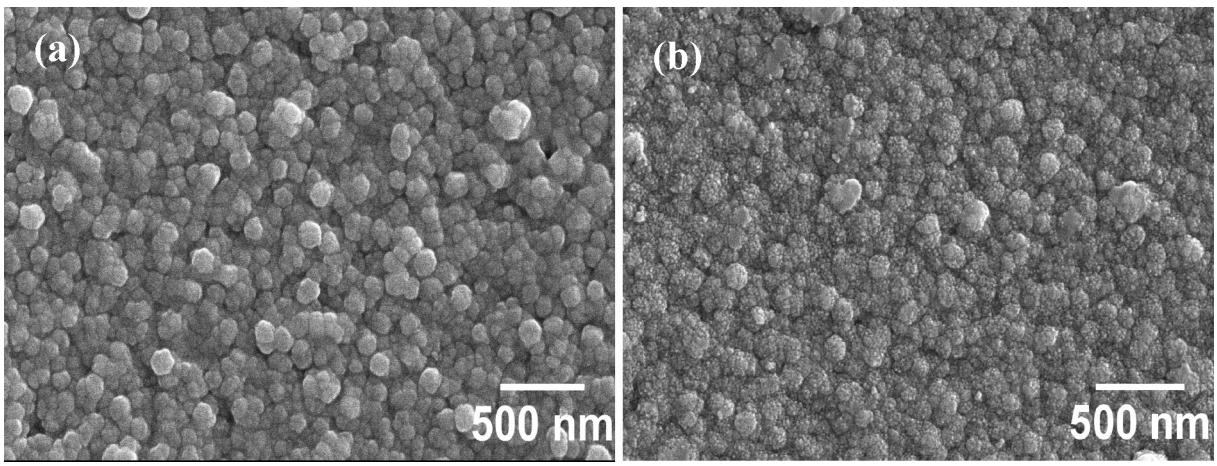

Fig. 8 Surface morphology of **a** bare CBD-CdS. **b** CBD-CdS/ED-CdTe* (S 40.)

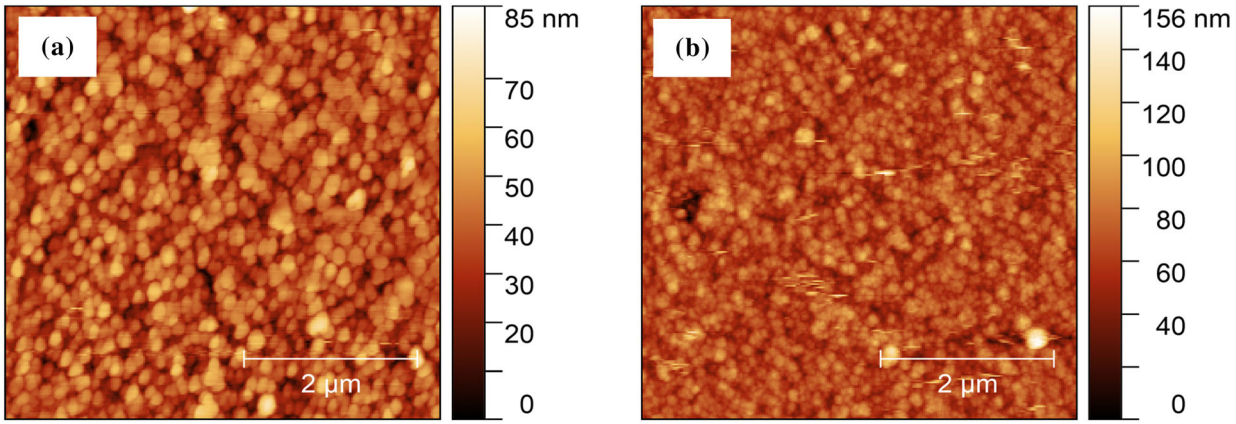

Fig. 9 AFM analysis of **a** bare CBD-CdS. **b** CBD-CdS/ED-CdTe* (S 40)

Table 4 Device performance of glass/CBD-CdS/CSS-CdTe and glass/CBD-CdS/ED-CdTe* (40 s)/CSS-CdTe after the $CdCl_2$ treatment

Sample	J_{SC} (mA/cm^2)	V_{OC} (V)	*FF* (%)	PCE (%)	R_s (Ω)	R_{sh} (Ω)
SC 0	38.1	0.737	52	14.6	54.7	908.9
SC 40	36.7	0.761	56	15.6	43.2	1436.0

3.5 Advancement of the device performance by $CdCl_2$ treatment

The device performances after the $CdCl_2$ treatment of the solar cells with no nucleation layer, glass/CBD-CdS/CSS-CdTe, and with the nucleation layer, glass/CBD-CdS/ED-CdTe* (40 s)/CSS-CdTe are shown in Table 4. Figure 10 shows the J–V curves for these two devices. The performances of the devices were drastically improved by the $CdCl_2$ treatment. Herein, the *FF*, and the V_{OC} of the devices were increased, and the resultant device efficiencies were 14.6% and 15.6% for the CBD-CdS/CSS-CdTe and CBD-CdS/ED-CdTe*(40 s)/CSS-CdTe, respectively.

After the $CdCl_2$ treatment, the conductivity type of the CSS-CdTe material (p-type) remained unchanged and showed 36.4% Cd and 63.6% Te in its composition measured by XRF. Herein, the Cd concentrations of the CdTe material was higher than the non-treated samples (25.4% Cd & 74.6% Te), which may affect the conductivity type of the CdTe material to some extent. The conductivity type of the CdTe is an important property of the cell as it influences the energy band diagrams, as shown in Figs. 11 and 12. Figure 11 gives the theoretical energy band gap for the n-CdS/p-CdTe junction, and Fig. 12 for the n-CdS/n-CdTe junction in different Fermi level positions in n-CdTe material. Here, the electron affinity (χ) of CdS was 4.5 eV [26], and that of CdTe

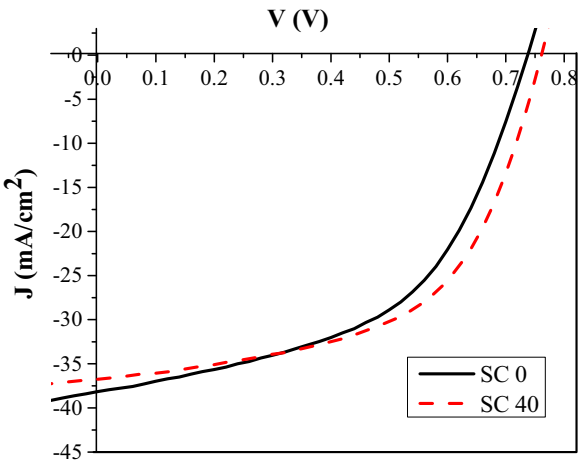

Fig. 10 J–V curves for devices SC 0 and SC 40 after the $CdCl_2$ treatment

was 4.28 eV [26, 27] while the energy band gap (E_g) observed for CdS, and CdTe was 2.39 eV and 1.49 eV, respectively. Therefore, $\Delta E_C = \chi_{CdS} - \chi_{CdTe} = 0.25$ eV.

When the Fermi level of the n-CdTe occurs below the Fermi level of n-CdS (Fig. 12a), the n-CdS/n-CdTe junction creates a band bending (Fig. 12b) without any obstruction for electron or hole transport. Similarly, if the Fermi level of the n-CdTe line-up above the Fermi level of n-CdS (Fig. 12c), the n-CdS/n-CdTe junction produces a discontinuity in the band bending, as shown in Fig. 12d. Therefore, the Fermi level difference ($\Delta E_{F\text{-}CdTe}$) of the n-CdTe

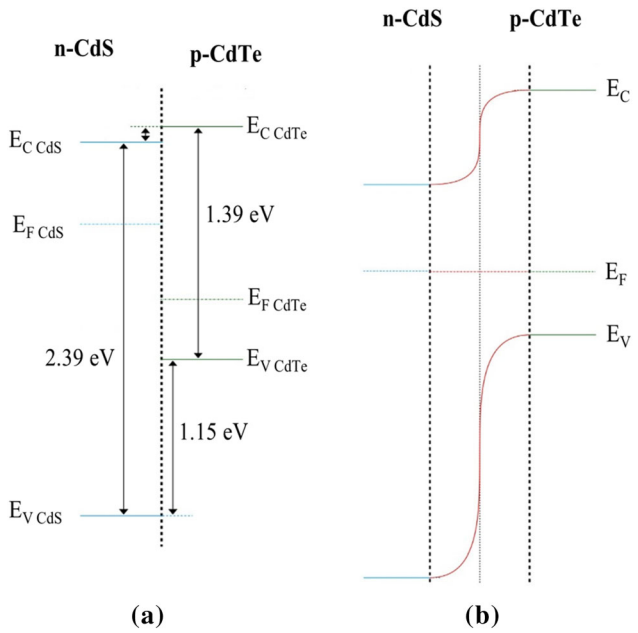

Fig. 11 Energy band diagram of n-CdS/p-CdTe **a** before the p–n junction formation and **b** band bending at the junction

should be greater than the total energy of the Fermi level difference of CdS ($\Delta E_{F\text{-}CdS}$) and 0.25 eV.

When considering the CdTe and back contact (Cu) interface, if the Fermi level (E_F) is greater than the work function of the back contact metal (ϕ_m), ($E_{F\text{-}} < \phi_m$), it creates a Schottky junction expediting the electron flow through the device [28]. If $E_F > \phi_m$ builds an ohmic contact, the conduction band edge at the CdTe and metal interface turns downward, increasing the electron flow in reverse and reducing the device's forward current density. Further, if $E_{F\text{-}} = \phi_m$, there is no band bending at the CdTe and metal interface edge, and it does not obstruct the electron flow. Therefore, band gap tuning in the absorber CdTe is highly crucial in improving the device performance of the CdS/CdTe solar cell fabrication. In this study, even though the conductivity type of CdTe remains as p-type after the $CdCl_2$ treatment, it may have slightly reduced p-type conductivity over the untreated cells and hence form a better Schottky junction between back contact and CdTe. This might explain the improved performance of the cells after the $CdCl_2$ treatment resulted from grain enhancement and Fermi level positioning. In addition, the ED-CdTe* nucleation layer tends to improve the device performance by reducing pinholes, thus forming better contact with the CSS-CdTe layer.

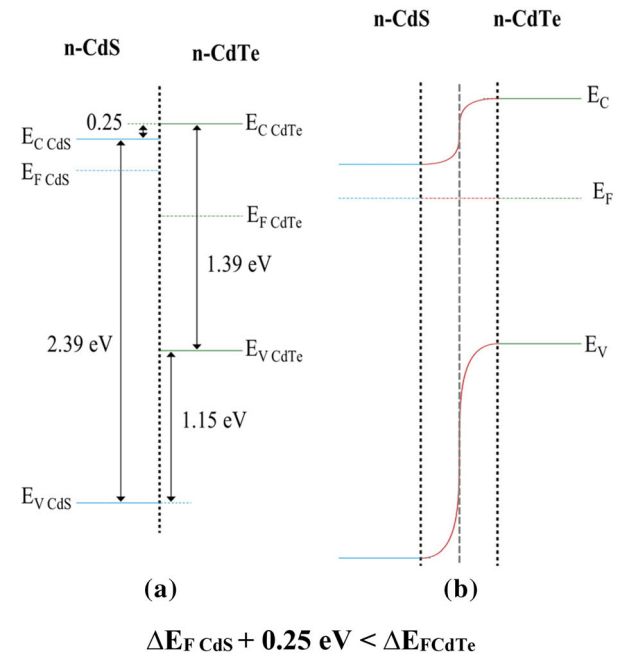

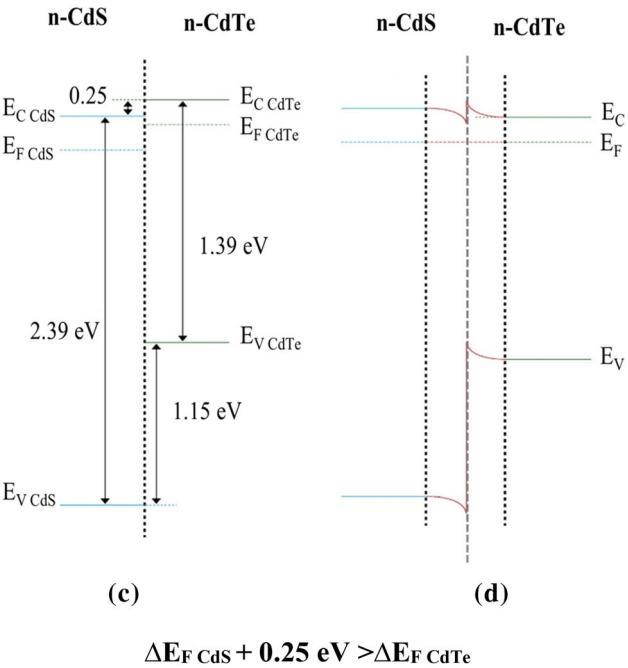

Fig. 12 Energy band diagram of n-CdS/n-CdTe **a** and **c** before the n–n junction formation, **b** and **d** band bending of the junction under two different Fermi level positions in n-CdTe

4 Conclusion

The CdTe nucleation layer implantation prior to depositing the CdTe absorber layer on the CdS layer in CdS/CdTe solar cells was discussed here. The

optimal thickness of the ED-CdTe* layer was identified by varying the electrodeposition time from 20 to 60 s. Among them, 40 s was identified as the optimal time of electrodeposition of the ED-CdTe* nucleation layer. Therein, the produced sample has shown the highest efficiency, the highest spectral response in the wavelength range of 400–850 nm, and the lowest ideality factor among the samples tested. This modified CBD-CdS/ED-CdTe*/CSS-CdTe solar cell delivered an efficiency of 9.12%, and after $CdCl_2$ treatment, efficiency reached 15.6%, which was a 13% improvement from the solar cell without a nucleation layer. The cell parameters in the optimal device were V_{OC} = 640 mV, 761 mV J_{SC} = 30.3 mA/cm^2, 36.7 mA/cm^2, and FF = 47%, 56% before and after the $CdCl_2$ treatment, respectively. Further, it has shown an ideality factor of 2.28 by the J-V curve in the dark and a reverse saturated current density of 6.65×10^{-5} mA/cm^2. Accordingly, the SC 40 has shown a minimum recombination effect. The optical transmittance data of S 40 reveals the ability of its nucleation layer to transmit more than 80%, and the band gap shrinkage was negligible. Additionally, SEM and AFM analysis verified the formation of an ultrathin ED-CdTe* nucleation layer in SC 40. Hence, implanting a nucleation layer before depositing the absorber layer is advantageous in manufacturing CdS/CdTe solar cells.

Acknowledgements

This work was supported by the State Ministry of Higher Education, Research and Innovation, Sri Lanka, under the Edu-Training program on Prototype Manufacturing of Solar Panels, the University Grants Commission of Sri Lanka—Innovation Grant, Sivananthan Laboratories INC, USA and L.B.D.R.P. Wijesundera and his research group.

Author contributions

G.K.U.P.G: Conception and design, investigation, interpretation and data analysis, writing and editing. A.A.I.L: CSS experiments, writing and editing. D.S.M.DeS: Supervision, funding acquisition, interpretation, writing, review, critical feedback and editing. B.S.D: Review, critical feedback and editing.

Funding

State Ministry of Higher Education,Research and Innovation,Sri Lanka,under the Edu-Training program on Prototype Manufacturing of Solar Panels,University Grants Commission of Sri Lanka—Innovation Grant

Data availability

The datasets analysed during the current study are available from the corresponding author upon reasonable request.

Declarations

Competing interests The authors have no relevant financial or non-financial interests to disclose.

References

1. S. Sundaram, K. Shanks, H. Upadhyaya, *A comprehensive guide to solar energy systems* (Elsevier, Amsterdam, 2018), pp.361–370
2. S. Rühle, Sci. Sol. Energy **130**, 139–147 (2016)
3. Photovoltaic Solar Energy Department National Renewable Energy Center (CENER), First Solar CdTe Photovoltaic Technology: Environmental, Health and Safety Assessment Final Report (2013)
4. M.A. Green, Y. Hishikawa, E.D. Dunlop, D.H. Levi, J. Hohl-Ebinger, M. Yoshita, A.W.Y. Ho-Baillie, Prog. Photovoltaics Res. Appl. **27**, 3 (2019)
5. O.K. Echendu, F. Fauzi, A.R. Weerasinghe, I.M. Dharmadasa, Thin Solid Films **556**, 529 (2014)
6. A.A.I. Lakmal, R.K.K.G.R.G. Kumarasinghe, V.A. Seneviratne, J.Y. Chen, J.M. Song, B.S. Dassanayake, Mater. Sci. Eng. B Solid-State Mater. Adv. Technol. **273**, 115406 (2021)
7. R.W.B.B.E. McCandless, I. Youm, Prog. Photovoltaics Res. Appl. **7**, 21 (1999)
8. C.H. Vásquez, J.M.F. Max, M.L. Albor Aguilera, M.A. González Trujillo, S.G.H.D. Jiménez Olarte, A.C. Orea, Mater. Res. Express **4**(1), 2–1 (2017)
9. J.D. Major, R. Tena-Zaera, E. Azaceta, L. Bowen, K. Durose, Sol. Energy Mater. Sol. Cells **160**, 107 (2017)
10. G. Kartopu, D. Turkay, C. Ozcan, W. Hadibrata, P. Aurang, S. Yerci, H.E. Unalan, V. Barrioz, Y. Qu, L. Bowen, A.K. Gürlek, P. Maiello, R. Turan, S.J.C. Irvine, Sol. Energy Mater. Sol. Cells **176**, 100 (2018)

11. G.K.U.P. Gajanayake, D.S.M. De Silva, H.Y.R. Atapattu, Mater. Sci. Eng. B Solid-State Mater. Adv Technol. **265**, 114952 (2021)
12. H.Y.R. Atapattu, D.S.M. De Silva, K.A.S. Pathiratne, I.M. Dharmadasa, J. Mater. Sci. Mater. Electron. **29**, 6236 (2018)
13. J. Lee, H. Ryu, D. Lim, K. Yang, W. Choi, J. Yi, Conf. Rec. IEEE Photovolt. Spec. Conf. **35**, 1927 (2010)
14. I.M. Dharmadasa, O.K. Echendu, F. Fauzi, N.A. Abdul-Manaf, O.I. Olusola, H.I. Salim, M.L. Madugu, A.A. Ojo, J. Mater. Sci. Mater. Electron. **28**, 2343 (2017)
15. I.M. Dharmadasa, *Advances in thin-film solar cells*, 2nd edn. (Jenny Stanford Publishing, New Delhi, 2018)
16. E.L. Meyer, Int. J. Photoenergy **2017**, 9 (2017)
17. S.M. Iftiquar, J. Yi, J. Electr. Eng. Technol. **11**, 939 (2016)
18. S. Hubbard, Photovoltic solar energy, in *Fundamentals to applications*. ed. by P. Verlinden, W. van Sark, A.F. Angèle Reinders (Wiley & Sons, Newyork, 2017), pp.39–46
19. S.J. Fonash, *Solar Cell Device Physics*, 2nd edn. (Elsevier Inc., Burlington, 2010)
20. I.M. Dharmadasa, A.E. Alam, A.A. Ojo, O.K. Echendu, J. Mater. Sci. Mater. Electron. **30**, 20330 (2019)
21. I.M. Dharmadasa, N.D.P.S.R. Kalyanaratne, R. Dharmadasa, J. Natl. Sci. Found. Sri Lanka **41**, 73 (2013)
22. I.M. Dharmadasa, M.L. Madugu, O.I. Olusola, O.K. Echendu, F. Fauzi, D.G. Diso, A.R. Weerasinghe, T. Druffel, R. Dharmadasa, B. Lavery, J.B. Jasinski, T.A. Krentsel, G. Sumanasekera, Coatings **7**, 0 (2017)
23. B. Qi, D. Kim, D.L. Williamson, J.U. Trefny, J. Electrochem. Soc. **143**, 517 (1996)
24. T. Baines, L. Bowen, B.G. Mendis, J.D. Major, A.C.S. Appl, Mater. Interfaces **12**, 38070 (2020)
25. B.S. Richards, K.R. McIntosh, Prog. Photovoltaics Res. Appl. **15**, 27 (2007)
26. H. Fardi, F. Buny, Int. J. Photoenergy (2013). https://doi.org/10.1155/2013/576952
27. A. Arce-Plaza, F. Sánchez-Rodriguez, M. Courel-Piedrahita, O. Vigil Galán, V. Hernandez-Calderon, S. Ramirez-Velasco, M. Ortega López, Coatings Thin-Film Technol. (2019). https://doi.org/10.5772/intechopen.79578
28. I.M. Dharmadasa, Coatings **4**, 282 (2014)